Article

Neuron

NMDA Receptors Enhance Spontaneous Activity and Promote Neuronal Survival in the Developing Cochlea

Highlights

- IHC-SGN synapses in the developing cochlea contain functional NMDARs
- NMDARs promote Ca^{2+} influx in SGN dendrites and increase repetitive firing
- NMDARs enhance coincident activation of neighboring SGNs during spontaneous events
- NMDAR signaling promotes survival of SGNs in vitro and in vivo

Authors

YingXin Zhang-Hooks, Amit Agarwal, Masayoshi Mishina, Dwight E. Bergles

Correspondence

dbergles@jhmi.edu

In Brief

Zhang-Hooks et al. find that NMDARs play a crucial role in development of the cochlea. By prolonging synaptic excitation at IHC-SGN synapses, NMDARs enhance repetitive firing of SGNs, increase dendritic Ca^{2+} influx, and promote SGN integration into the auditory pathway.

Zhang-Hooks et al., 2016, Neuron *89*, 337–350
January 20, 2016
http://dx.doi.org/10.1016/j.neuron.2015.12.016

CellPress

Neuron
Article

NMDA Receptors Enhance Spontaneous Activity and Promote Neuronal Survival in the Developing Cochlea

YingXin Zhang-Hooks,[1] Amit Agarwal,[1] Masayoshi Mishina,[2] and Dwight E. Bergles[1,*]
[1]Solomon H. Snyder Department of Neuroscience, Johns Hopkins University School of Medicine, Baltimore, MD 21205, USA
[2]Brain Science Laboratory, the Research Organization of Science and Technology, Ritsumeikan University, Shiga 525-8577, Japan
*Correspondence: dbergles@jhmi.edu
http://dx.doi.org/10.1016/j.neuron.2015.12.016

SUMMARY

Spontaneous bursts of activity in developing sensory pathways promote maturation of neurons, refinement of neuronal connections, and assembly of appropriate functional networks. In the developing auditory system, inner hair cells (IHCs) spontaneously fire Ca^{2+} spikes, each of which is transformed into a mini-burst of action potentials in spiral ganglion neurons (SGNs). Here we show that NMDARs are expressed in SGN dendritic terminals and play a critical role during transmission of activity from IHCs to SGNs before hearing onset. NMDAR activation enhances glutamate-mediated Ca^{2+} influx at dendritic terminals, promotes repetitive firing of individual SGNs in response to each synaptic event, and enhances coincident activity of neighboring SGNs that will eventually encode similar frequencies of sound. Loss of NMDAR signaling from SGNs reduced their survival both in vivo and in vitro, revealing that spontaneous activity in the prehearing cochlea promotes maturation of auditory circuitry through periodic activation of NMDARs in SGNs.

INTRODUCTION

Synapses between inner hair cells (IHCs) and spiral ganglion neurons (SGNs) in the mammalian cochlea transform IHC activity into action potentials to enable perception of sound. In altricial animals, these synapses are formed during late embryonic development and become functional several weeks before hearing onset (Beutner and Moser, 2001). Bursts of synaptic activity are induced during this pre-hearing period through periodic excitation of IHCs by mechanisms intrinsic to the cochlea (Johnson et al., 2011; Tritsch et al., 2007), resulting in IHC Ca^{2+} spikes, glutamate release, and ultimately bursts of action potentials in SGNs that are carried to the CNS by auditory nerve fibers. Spontaneous burst firing is a common feature of developing sensory pathways (Blankenship and Feller, 2010) that has been implicated in promoting the survival of sensory neurons, refining their projections in the CNS, and initiating maturation of target neurons (Kirkby et al., 2013); however, little is known about how developing synapses shape this activity and contribute to formation of sensory pathways.

In the developing cochlea, SGNs fire action potentials in a highly stereotyped sequence within each burst, with spikes clustered into discrete mini-bursts consisting of multiple action potentials (Tritsch et al., 2010). Each mini-burst is induced by a single Ca^{2+} spike in the presynaptic IHC, indicating that these nascent ribbon synapses are capable of remarkable signal amplification at this early stage of development. The repetitive firing of SGNs may enable signals to propagate more efficiently through the auditory pathway, induce long-term synaptic plasticity (Tzounopoulos et al., 2004), and promote activity-dependent synaptic refinement (Clause et al., 2014). At central synapses, NMDA receptors (NMDARs) enhance postsynaptic depolarization due to their slow deactivation kinetics (Cull-Candy and Usowicz, 1987), suggesting that they could promote synaptic amplification in the developing cochlea to facilitate neuronal integration. NMDAR subunit expression has been detected in adult SGNs by in situ hybridization and immunocytochemistry (Niedzielski and Wenthold, 1995; Safieddine and Eybalin, 1992; Usami et al., 1995), and pharmacological manipulation of NMDARs in the cochlea of adult mice alters the firing of auditory neurons (Felix and Ehrenberger, 1990; Puel et al., 1991). However, the contribution of NMDARs to synaptic excitation of SGNs prior to hearing onset remains uncertain. Although NMDAR subunit expression has been detected in SGNs at this age (Knipper et al., 1997; Lu et al., 2011), synaptic currents recorded directly from SGN dendrites in conditions favorable for NMDAR activation are blocked by selective AMPAR antagonists (Glowatzki and Fuchs, 2002; Grant et al., 2010), suggesting that they may be excluded from synapses. NMDAR-mediated currents can be elicited in SGNs in prehearing cochleae after exposure to salicylate (Peng et al., 2003; Ruel et al., 2008), a non-steroidal anti-inflammatory drug that induces tinnitus, suggesting that there is a latent pool of NMDARs in developing SGNs that can be mobilized by particular chemical stimuli.

Here, we show that functional NMDARs are expressed by SGNs prior to hearing onset and that they play a prominent role in controlling both synaptic excitation and the coincidental activation of neighboring SGNs during spontaneous activity. Synaptic currents recorded directly from SGNs in prehearing cochleae were biphasic, reflecting activation of both AMPA and NMDARs. NMDAR activation prolonged synaptic currents,

enhanced Ca^{2+} influx, and stimulated the repetitive firing of SGNs. Conversely, pharmacological or genetic disruption of NMDAR signaling in SGNs accelerated synaptic currents, reduced the overall activity and correlated firing of SGNs, and impaired their survival. Together, these studies reveal that NMDARs enhance the gain of synapses in the developing cochlea and promote integration of SGNs into the auditory pathway.

RESULTS

Type I SGNs Express Functional NMDARs

To determine if SGNs in the developing cochlea express functional NMDARs, we isolated cochleae from postnatal day (P) 5–7 rats and made whole-cell recordings from SGN somata (Figures 1A and 1B). These cells exhibited physiological and anatomical characteristics of type I SGNs (Jagger and Housley, 2002); they had a resting membrane potential of −60 to −80 mV and exhibited anomalous rectification when hyperpolarized and rapid spike frequency adaptation when depolarized (Figure 1C). Histological analysis revealed that they had a bipolar morphology (Figure 1D) and extended a single dendrite that terminated near the base of one IHC (Figures 1E–1G). When voltage-clamp recordings were performed in conditions optimized to detect NMDAR activity (Mg^{2+}-free and D-serine containing artificial cerebrospinal fluid [ACSF], V_m = −70 mV), small inward current fluctuations were visible (Figures 1H and 1I) that were blocked by the NMDAR antagonist CPP (Figures 1J and 1K) and enhanced when glutamate uptake was inhibited with TBOA (Figures 1L and 1M), indicating that these fluctuations arise from periodic activation of NMDARs by ambient glutamate (Sah et al., 1989). Focal application of NMDA to the soma of SGNs elicited transient inward currents that were also inhibited by CPP (Figures 1N and 1O), indicating that functional NMDARs are present in the somatic membrane of these neurons.

To assess whether NMDARs are localized to IHC-SGN synapses, glutamate receptor agonists were applied directly to SGN dendritic terminals near the base of IHCs (Figure 2A), where these synapses reach their highest density (Safieddine et al., 2012). As shown by the spread of the fluorescent dye Alexa 488, which was included in the puffer pipette (Figure S1A), agonist application was restricted to the region around IHCs (dye spread: 75 ± 15 μm, n = 5 cochleae) and did not reach the spiral ganglion (IHC-SGN distance: 330 ± 6 μm, n = 3 cochleae). Application of AMPAR agonists kainate or glutamate to SGN dendritic terminals elicited trains of action potentials that persisted when IHC Ca^{2+} channels were inhibited with nifedipine but were blocked by AMPAR antagonists GYKI 53655 or NBQX (Figure 2A; n = 11 cells), indicating that this manipulation induces SGN firing through direct stimulation of postsynaptic glutamate receptors rather than depolarization of presynaptic IHCs. Focal application of NMDAR agonists NMDA or D-aspartate also induced trains of action potentials that persisted when AMPARs were blocked by GYKI 53655 but were abolished by NMDAR antagonists MK-801 or CPP (Figure 2B). Moreover, when current clamp recordings were made from SGNs, focal application of glutamate receptor agonists induced transient depolarizations that triggered SGN firing (Figure S1B); when recordings were performed in the presence of tetrodotoxin (TTX) to block action potentials, NMDAR agonist application elicited depolarizations that were inhibited by CPP (Figures 2C and 2D). These results indicate that NMDARs are present in SGN dendrites at a density sufficient to trigger action potentials.

NMDARs Prolong the Time Course of IHC-SGN Synaptic Currents and Enhance Synaptic Depolarization

NMDARs can markedly enhance excitatory postsynaptic currents (EPSCs) due to their slow kinetics and large unitary conductance (Cull-Candy and Usowicz, 1987). Although NMDAR-mediated postsynaptic currents were not observed in previous studies when EPSCs were recorded directly from SGN dendritic boutons (Glowatzki and Fuchs, 2002; Grant et al., 2010; Seal et al., 2008), these receptors are labile, and NMDAR-mediated currents often disappear rapidly in whole-cell recordings (Káradóttir et al., 2005; MacDonald et al., 1989; Rosenmund and Westbrook, 1993). To minimize possible disruption of postsynaptic receptors, we recorded spontaneous EPSCs (sEPSCs) remotely from SGN somata (Figure 3A). When voltage-clamp recordings were performed in TTX, transient inward currents could be resolved that exhibited a time course similar to miniature EPSCs (mEPSCs) in central neurons (Goforth et al., 2011; Savić et al., 2003). These events were blocked by NBQX and CPP (Figures 3B and 3D), indicating that they resulted from glutamatergic transmission. When recordings were performed in the absence of extracellular Mg^{2+} to allow current flow through NMDARs at negative potentials (V_m = −70 mV), sEPSCs had a conspicuously prolonged time course (Figure 3B). Addition of CPP lowered the baseline noise, accelerated the decay time of sEPSCs by 53%, and reduced their charge transfer by 48%, without affecting their frequency or rise time (Figures 3B–3D). The characteristically slow kinetics of the NMDAR current was apparent after subtracting the average sEPSC in CPP from control (Figure 3C), which is comparable to NMDAR-mediated currents recorded at individual glutamatergic synapses in the CNS (Gideons et al., 2014; Goforth et al., 2011; Savić et al., 2003).

To determine how NMDAR activation alters the time course of SGN membrane depolarization, we also performed current clamp recordings from SGN somata (Figure 3E). In 0 mM Mg^{2+} ACSF containing TTX, spontaneous excitatory postsynaptic potentials (sEPSPs) were visible that had a prolonged decay (Figures 3F and 3G). Inhibition of NMDARs with CPP reduced the duration of these events by 79%, demonstrating the profound effect that NMDAR activation can have on membrane potential changes due to their slow deactivation kinetics. NMDAR inhibition did not change the frequency or rise time of sEPSPs but reduced the peak amplitude by 38% and the envelope of depolarization (estimated by integrating the area under each event) by 74% (Figure 3H). Moreover, when whole-cell recordings were performed in NBQX, spontaneous inward currents and membrane depolarizations that exhibited slow rise and decay kinetics were visible (Figures S2A and S2D). Application of NBQX produced effects on synaptic events that were complimentary to CPP (compare to Figure 3), reducing their peak amplitude and slowing their rise times without changing their frequency or decay kinetics (Figure S2). It was not possible to distinguish single from double or multiple release events (Rutherford et al.,

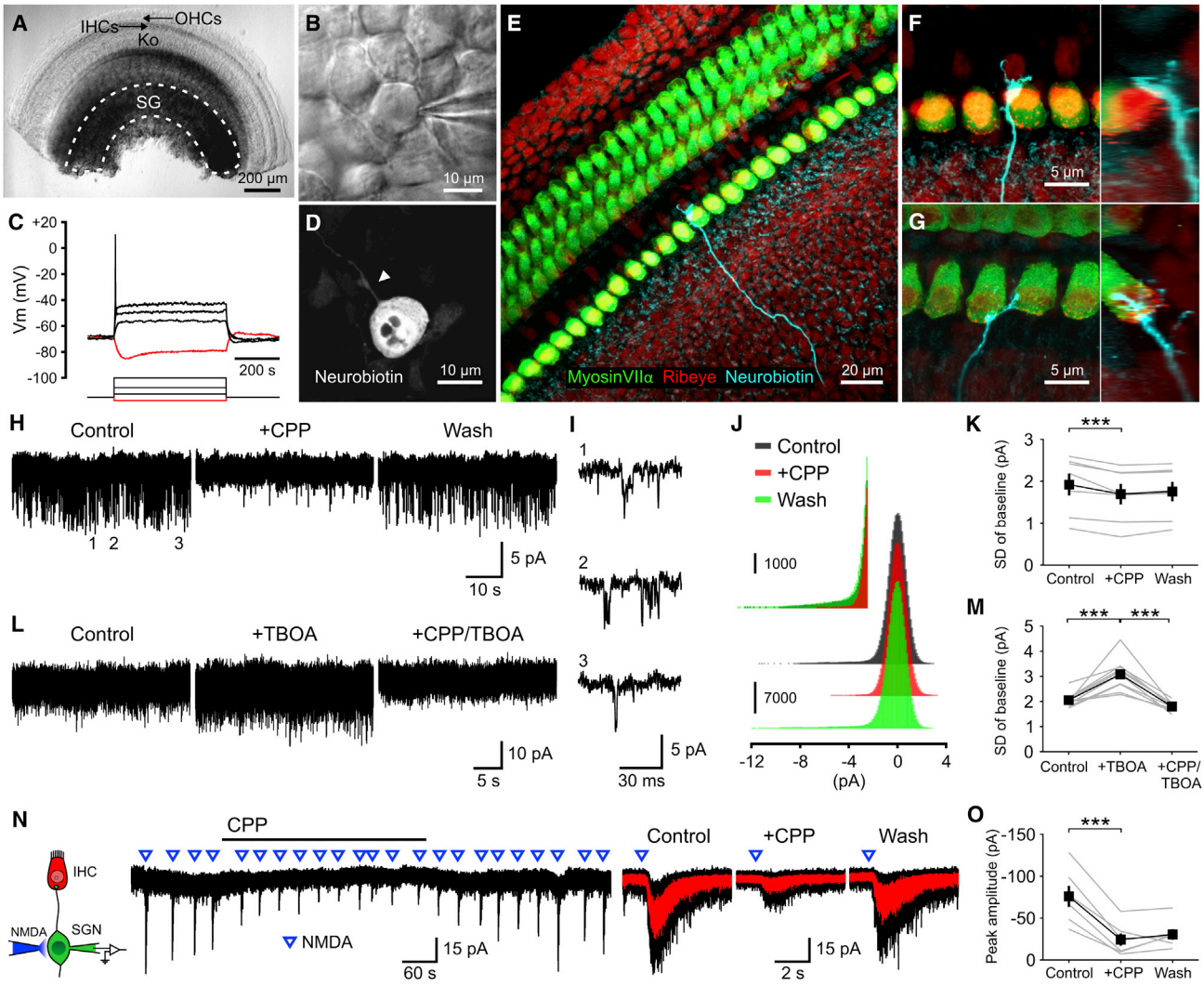

Figure 1. NMDARs Are Expressed by SGNs

(A) Middle turn of a P5 rat cochlea. Dashed line outlines the spiral ganglion (SG). OHCs, outer hair cells; IHCs, inner hair cells; Ko, Kölliker's organ.

(B) Somata of a SGN during a juxtacellular recording.

(C) Membrane responses of a SGN to current injections. Red trace, injection of −20 pA; black traces, injections of 20, 60, and 120 pA.

(D) Somata of a SGN filled with neurobiotin during a whole-cell recording. Arrowhead highlights the single dendritic process.

(E–G) Dendrites of SGNs filled with neurobiotin. Orthogonal views are shown to the right. Terminals were located on either the abneural (F) or neural (G) side of IHCs.

(H and L) Baseline noise during whole-cell voltage-clamp recordings from SGNs in 0 Mg^{2+} ACSF (V_m = −70 mV). [CPP], 20 μM; [TBOA], 50 μm.

(I) Three examples of individual channel activity from the recording shown in (H).

(J) Amplitude histogram of the baseline noise recording shown in (H). Inset shows the amplitude histogram for inward current fluctuations at an expanded scale.

(K and M) Plots of the SD of current fluctuations. n = 7 (K) and 10 (M) cells; one-way repeated-measures ANOVA followed by Tukey's test; ***p < 0.001. Data show average values from each cell (gray) and mean ± SEM for all cells (black).

(N) Left: Diagram of the recording configuration. Middle: Inward currents triggered by focal applications of NMDA (100 ms, 0.5 mM) in the presence of TTX (1 μM). Right: Average responses to NMDA (red) superimposed on individual responses (black).

(O) Plot of the average peak amplitude of current induced by NMDA in control, + CPP, and wash conditions. n = 6 cells; one-way repeated-measures ANOVA followed by Tukey's test; ***p < 0.001. Data show average values from each cell (gray) and mean ± SEM for all cells (black).

2012) in these recordings, because of the slow and variable waveform of NMDAR-mediated synaptic events. Therefore, all events were analyzed in both control and + NBQX conditions, resulting in average responses that have longer decay times, increased charge transfer, and depolarization areas compared to the kinetics of CPP-sensitive components (Figure 3) compiled from unitary events.

NMDAR channel opening is enhanced at higher pH (Tang et al., 1990), in contrast to other ionotropic glutamate receptors that are largely insensitive to pH changes within a physiological

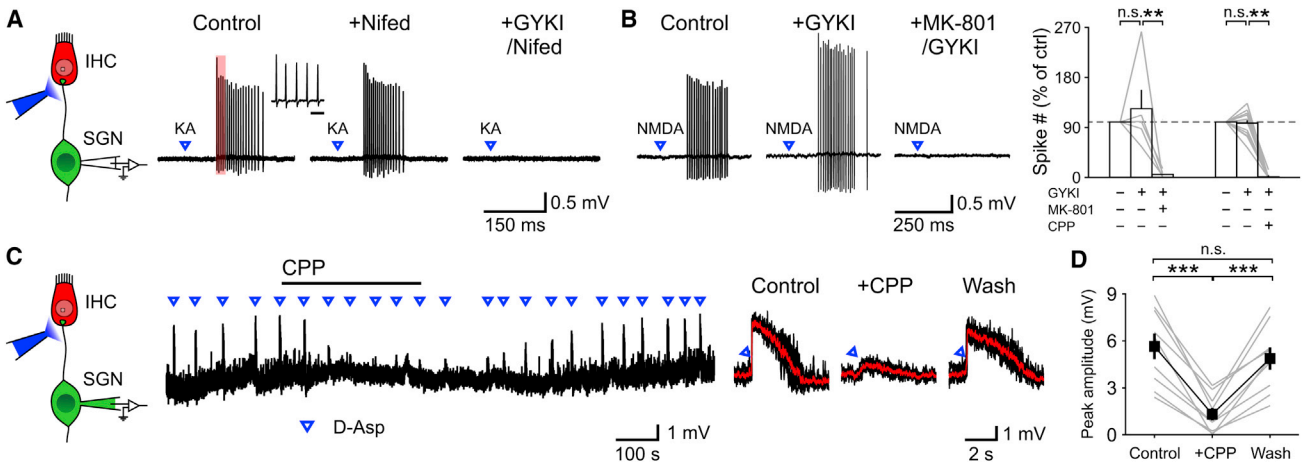

Figure 2. NMDARs Are Present at SGN Dendritic Terminals

(A) Left: Diagram of the recording configuration. Right: Juxtacellular recording from a SGN showing responses to focal applications of kainate (KA) (10 ms, 100 μM) in control, nifedipine (Nifed) (50 μM) and GYKI53655 (GYKI) (100 μM) + Nifed conditions. Inset shows the first five action potentials in the train (region delimited by red rectangle) at an expanded timescale. Scale bar, 5 ms.

(B) Left: Juxtacellular recording from a SGN showing responses to focal applications of NMDA (10 ms, 1 mM) in control, GYKI, and MK-801 (50 μM) + GYKI conditions. Right: Plot of the number of action potentials elicited by NMDA in various drug conditions. MK-801, n = 5 cells, one-way repeated-measures ANOVA followed by Tukey's test; CPP (20 μM), n = 13 cells, Friedman's ANOVA followed by Dunn's test; n.s., not significant, $p \geq 0.05$; **$p < 0.01$. Data show average values from each cell (gray lines) and mean ± SEM for all cells (white bars).

(C) Left: Diagram of the recording configuration. Right: Whole-cell current clamp recording from a SGN showing depolarizations induced by focal applications of D-aspartate (D-Asp) (10 ms, 0.5 mM), an NMDAR agonist, in the presence of TTX (1 μM). Average responses (red) to D-aspartate superimposed on individual traces (black) in control, + CPP, and wash conditions are shown to the right.

(D) Plot of the average peak amplitude of depolarization induced by D-aspartate in control, + CPP, and wash conditions. n = 9 cells; one-way repeated-measures ANOVA followed by Tukey's test; n.s., not significant, $p \geq 0.05$; ***$p < 0.001$. Data show average values from each cell (gray) and mean ± SEM for all cells (black). See also Figure S1.

range. Acidification occurs at IHC afferent synapses due to proton release from synaptic vesicles (Cho and von Gersdorff, 2014), and exposure to sodium salicylate, a salt of a weak acid that renders solutions basic, has been reported to induce the appearance of NMDARs in SGNs (Ruel et al., 2008). An alkaline shift in pH from 7.3 to 8.3 (Figures S3A and S3B) increased the frequency of sEPSCs (Figure S3C), consistent with the effects of pH on presynaptic neurotransmitter release (Sinning and Hübner, 2013). At this elevated pH, the decay time of sEPSCs was increased by 11% and the charge transfer by 24% (Figures S3B and S3C), comparable to the effects of alkaline pH shifts on heterologously expressed NMDARs (Traynelis et al., 1995). Subsequent application of CPP shortened the decay time and reduced the charge transfer to levels comparable to that recorded at physiological pH (Figures 3D and S3C; pH 7.3 versus pH 8.3 + CPP: weighted tau of decay, p = 0.20; charge transfer, p = 0.66, two-sample t test). These findings provide independent evidence for the contribution of NMDARs to sEPSCs and suggest that acidification of the cochlea could impair the transfer of hair cell activity to SGNs by inhibiting NMDAR gating.

Sounds of different frequencies are encoded in the mammalian cochlea by distinct hair cells positioned in a tonotopic gradient along the organ of Corti, with their characteristic frequencies increasing from apex to base. Given the extreme demands of encoding high-frequency sounds, IHC-SGN synapses in the basal cochlea may contain fewer NMDARs to shorten the duration of synaptic excitation. Type I SGNs residing in this region also formed synapses with only one IHC (Figure S4A) and generated a single action potential upon depolarization (Figure S4B). Moreover, CPP reduced the decay time and charge transfer of sEPSCs comparable to those recorded from SGNs residing in the apical region (Figures S4C and S4D). Indeed, for sEPSCs recorded in both basal and apical regions, there was a positive correlation between the weighted tau of decay in control and the change of decay tau after CPP (Figure S4D; base, r = 0.94, p < 0.001; apex, r = 0.67, p < 0.05, Pearson's two-tailed test), as expected if NMDARs contribute to the slow time course of decay in sEPSCs in both regions.

NMDARs Promote Ca^{2+} Influx at IHC-SGN Synapses

NMDARs impact neuronal development by enhancing elevation of intracellular Ca^{2+} during neural activity (MacDermott et al., 1986; Papadia et al., 2005; Xia et al., 1996). To analyze Ca^{2+} signaling in individual SGN dendritic terminals, we developed a method to achieve sparse expression of the genetically encoded Ca^{2+} indicator GCaMP3 (Tian et al., 2009) in SGNs (Figure 4) using *Advillin*^{Cre} (*Avil*^{Cre}) mice (da Silva et al., 2011). We confirmed Cre activity in SGNs by crossing *Avil*^{Cre} mice with a conditional reporter line (Ai9, *R26-lsl-tdTomato*), which resulted in expression of tdTomato by only a subset of type I and type II SGNs with increasing density from apex to base (Figures 4A and 4B).

To determine if NMDAR activation contributes to postsynaptic Ca^{2+} influx in SGN dendritic terminals, we crossed *R26-lsl-GCaMP3* mice (Paukert et al., 2014) with *Avil*^{Cre} mice and

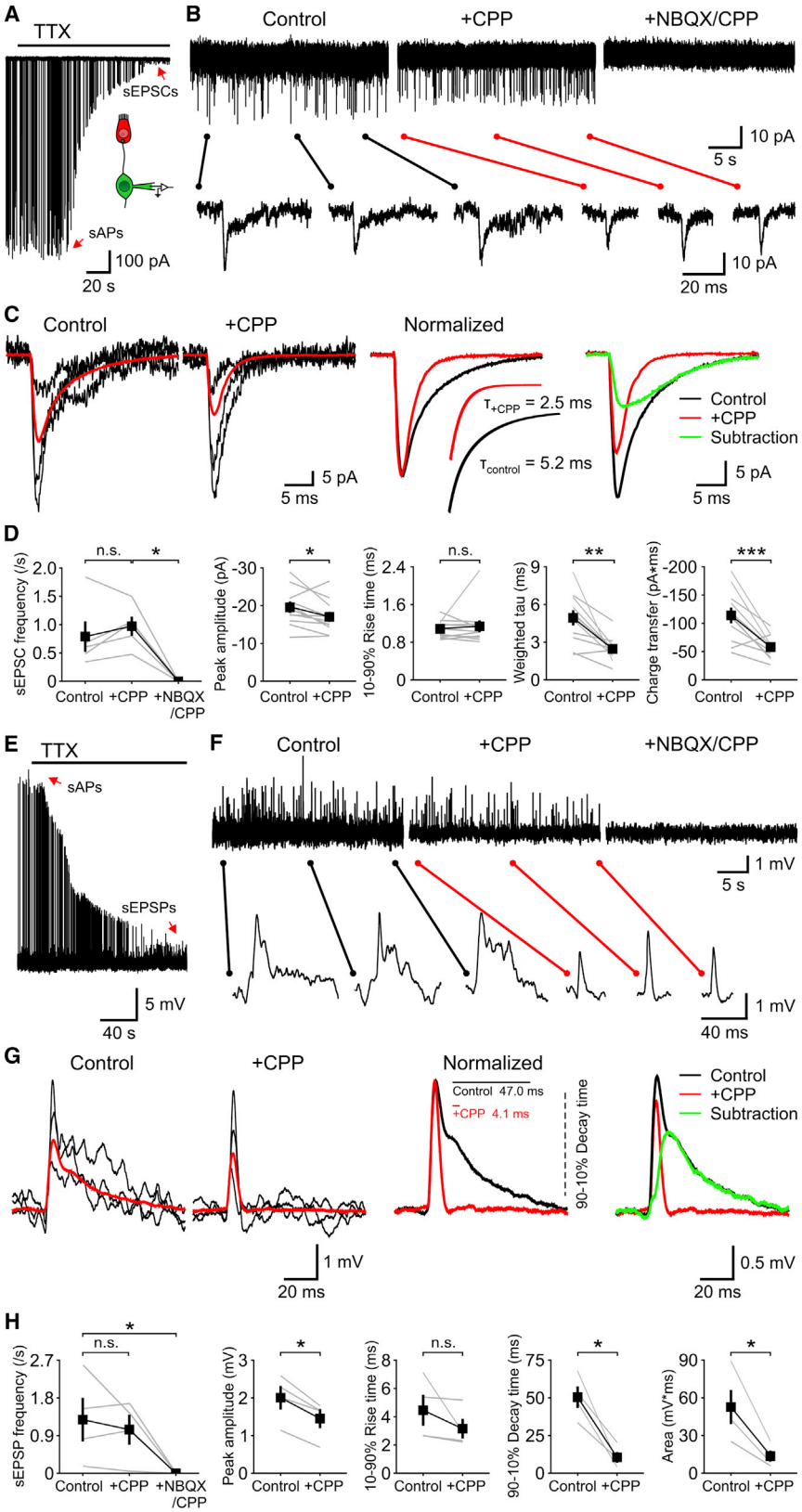

Figure 3. NMDAR Activation Prolongs Synaptic Currents and Depolarizations

(A) Voltage-clamp recording from a SGN showing synaptic currents that persist in 1 μM TTX (V_m = −70 mV). Inset shows the recording configuration. sAPs, spontaneous action potentials; sEPSCs, spontaneous excitatory postsynaptic currents.

(B) sEPSCs recorded from a SGN in control, CPP (20 μM), and in NBQX (20 μM) + CPP conditions (V_m = −70 mV, 0 Mg^{2+} ACSF with 1 μM TTX). Individual EPSCs are shown below at an expanded timescale.

(C) Left: Overlay of three representative sEPSCs (black) and average sEPSC (red) recorded in control and + CPP conditions. Middle: Average sEPSCs recorded in control (black) and + CPP (red) normalized to the peak. Inset shows double (control) and single (+ CPP) exponential fits for average sEPSC decay and weighted tau of decay (T). Right: Subtraction from the two average sEPSCs showing waveform of the CPP-sensitive current (green).

(D) Plots of sEPSC frequency (n = 5 cells, Friedman's ANOVA followed by Dunn's test), peak amplitude, 10%–90% rise time, weighted tau of decay, and charge transfer (n = 14 cells, paired-sample t test) in control; CPP; and NBQX + CPP conditions. n.s., not significant, $p \geq 0.05$; *$p < 0.05$; **$p < 0.01$; ***$p < 0.001$. Data show average values from each cell (gray) and mean ± SEM for all cells (black).

(E) Current clamp recording from a SGN showing synaptic depolarizations that persist in 1 μM TTX. sEPSPs, spontaneous excitatory postsynaptic potentials.

(F) sEPSPs recorded from a SGN in control, CPP (20 μM), and NBQX (20 μM) + CPP conditions (0 Mg^{2+} ACSF with 1 μM TTX). Individual EPSPs are shown below at an expanded timescale.

(G) Left: Overlay of three representative sEPSPs (black) and average sEPSP (red) recorded in control and + CPP conditions. Middle: Average sEPSPs recorded in control (black) and + CPP (red) normalized to the peak. Inset shows 90%–10% decay times. Right: Subtraction from the two average sEPSPs showing waveform of the CPP-sensitive depolarization (green).

(H) Plots of sEPSP frequency (Friedman's ANOVA followed by Dunn's test), peak amplitude, 10%–90% rise time, 90%–10% decay time, and area (paired-sample t test) in control; CPP; and NBQX + CPP conditions. n = 4 cells; n.s., not significant, $p \geq 0.05$; *$p < 0.05$. Data show average values from each cell (gray) and mean ± SEM for all cells (black).

See also Figures S2–S4.

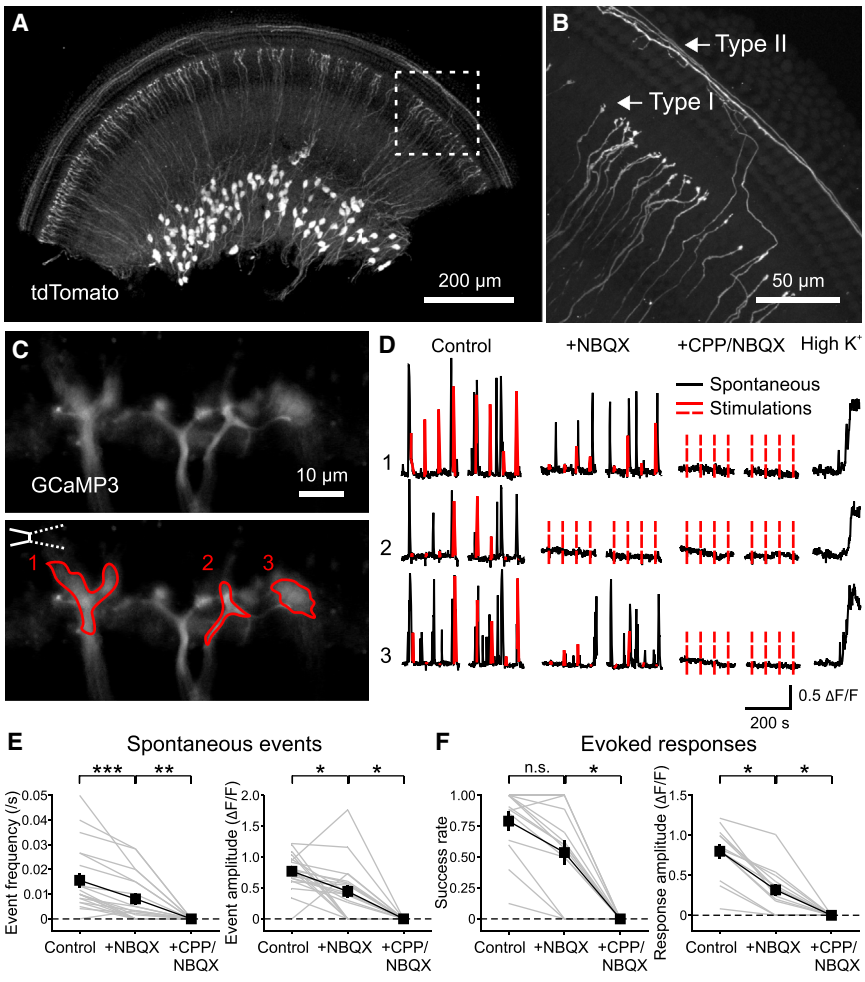

Figure 4. NMDAR Activation Enhances Ca^{2+} Influx at SGN Dendritic Terminals

(A) Middle turn of the cochlea from a P7 *Avil*^{Cre}; *R26-lsl-tdTomato* (termed as *Avil*^{Cre}; *tdT*) mouse showing expression of tdTomato. Apical direction is to the right.

(B) High magnification image of the area outlined in (A) showing individual dendrites of type I and type II SGNs.

(C) Ca^{2+} imaging from SGN dendritic terminals. Upper: Maximum intensity projection of individual SGN dendritic terminals near the base of IHCs from the cochlea of a P5 *Avil*^{Cre}; *R26-lsl-GCaMP3* (termed as *Avil*^{Cre}; *GCaMP3*) mouse, over 300 s Ca^{2+} imaging in the control condition. Lower: Same image showing the placement of a stimulation pipette applying high-sucrose ACSF near IHCs and regions of interest (ROIs) in three dendritic terminals to record Ca^{2+} signals.

(D) Ca^{2+} recordings of the ROIs from (C) in control, NBQX (20 µM), and CPP (20 µM) + NBQX conditions. Black traces are spontaneous activity; red traces are responses to stimulations; dashed red lines indicate absence of detectable responses to stimulations. High K^+ (10 mM) ACSF was applied at end of the experiment to assess responsiveness of GCaMP3.

(E and F) Plots of spontaneous event frequency and amplitude (E) (n = 20 terminals from 12 cochleae) and stimulation success rate and evoked response amplitude (F) (n = 13 terminals from 8 cochleae) in control, NBQX, and CPP + NBQX conditions. Friedman's ANOVA followed by Dunn's test; n.s., not significant, $p \geq 0.05$; *$p < 0.05$; **$p < 0.01$; ***$p < 0.001$. Dashed lines indicate 0 values. Data show values from individual terminals (gray) and mean ± SEM for all terminals (black).

See also Figure S5 and Movie S1.

cultured middle turns of P4–P6 cochleae to visualize dendritic Ca^{2+} transients (Figure 4C). In these cochleae, spontaneous Ca^{2+} transients were observed in groups of neighboring SGN dendritic terminals (Figure 4D; Movie S1), consistent with the synchronized activation of adjacent IHCs by ATP released from Kölliker's organ (Tritsch and Bergles, 2010; Tritsch et al., 2007). In the same preparation, deflecting the stereocilia of IHCs presynaptic to GCaMP3$^+$ terminals induced Ca^{2+} transients in SGN dendrites lasting several seconds (Figure 4C), comparable to spontaneous Ca^{2+} transients (half width: 4.5 ± 0.3 s for spontaneous, 4.0 ± 0.5 s for evoked events, n = 13 terminals, p = 0.28, paired-sample t test) (Figure 4D; Movie S1). In the majority of dendritic terminals (16/27), spontaneous Ca^{2+} transients persisted when AMPARs were blocked, although they were reduced in amplitude and frequency; in these terminals, all remaining activity was abolished by CPP (Figures 4D and 4E). Moreover, Ca^{2+} transients elicited in most SGN dendritic terminals (10/16) by stereocilia deflection were also inhibited by CPP (Figures 4D and 4F). This effect of CPP was specific to NMDARs in SGNs, as it did not alter the frequency or amplitude of inner supporting cell (ISC) spontaneous activity (Figures S5A–S5C) or affect the resting membrane potential or intrinsic excitability of IHCs (Figures S5D and S5E). These experiments demonstrate that activation of NMDARs at IHC-SGN synapses induces postsynaptic Ca^{2+} transients in dendritic terminals of most type I SGNs.

NMDARs Regulate SGN Firing Behavior

To determine if NMDARs regulate the stereotyped firing of SGNs during the prehearing period, we made juxtacellular recordings from SGN somata in cultured rat cochleae (to allow cells to recover from the trauma induced by isolation) and monitored their firing behavior during both spontaneous activity and in response to IHC depolarization evoked by focal application of high K^+ ACSF (Figure 5A). Application of NBQX and CPP abolished nearly all action potentials in SGNs (spontaneous spike rate reduced by 98%, n = 4 cells, $p < 0.05$; evoked spike rate reduced by 99%, n = 5 cells, $p < 0.01$, paired-sample t test), indicating that their activity arises primarily from glutamate-receptor-dependent synaptic activity. In ACSF containing physiological levels of Mg^{2+} (1.3 mM), the number of action potentials elicited in SGNs during spontaneous activity or by high K^+ application was markedly reduced by CPP (Figures 5B and 5C), even when applied at a lower concentration (Figure S6), suggesting

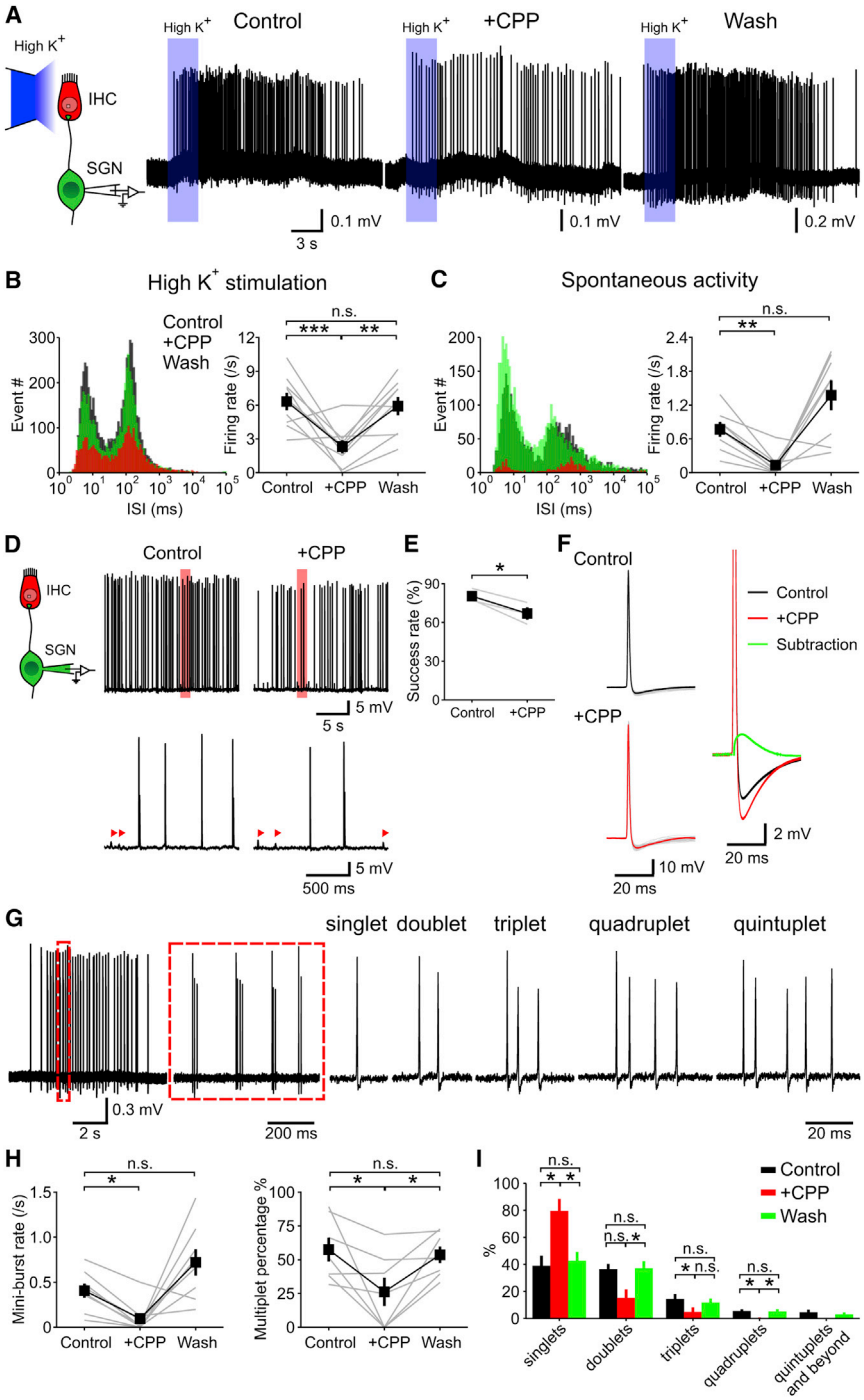

Figure 5. NMDAR Activation Increases SGN Activity and Promotes Repetitive Firing

(A) Left: Diagram of the recording configuration. Right: Juxtacellular recordings of action potentials from SGNs triggered by local applications (3 s, blue rectangles) of high K^+ (10 mM) solution to IHCs. [CPP], 20 μM.

(B and C) Analysis of SGN spontaneous (B) and evoked (C) firing. Left: Log-binned ISI histograms of action potentials in control, + CPP, and wash conditions (n = 9 [B] and 8 [C] cells). Right: Plots of the firing rate in control, + CPP, and wash conditions. One-way repeated-measures ANOVA followed by Tukey's test; n.s., not significant, $p \geq 0.05$; **$p < 0.01$; ***$p < 0.001$. Data show average values from each cell (gray) and mean ± SEM for all cells (black).

(D) Left: Diagram of the recording configuration. Right: Whole-cell current clamp recording from a SGN showing spontaneous action potentials in control and + CPP conditions. Regions delimited by red boxes are shown at an expanded timescale, with arrowheads highlighting sEPSPs that failed to generate action potentials.

(E) Plot of the success rate of EPSPs reaching firing threshold in control and + CPP conditions. n = 3 cells; paired-sample t test; *$p < 0.05$. Data show average values from each cell (gray) and mean ± SEM for all cells (black).

(F) Left: Overlay of individual action potentials (gray, 86 for control and 77 for + CPP condition) and average action potential waveforms recorded in control (black) and + CPP (red) conditions. Right: Subtraction from the two average action potentials showing waveform of the CPP-sensitive depolarization (green).

(G) Temporal pattern of SGN firing within spontaneous bursts. Left: Juxtacellular recording of a spontaneous burst of action potentials from a SGN. Region highlighted by the dashed red line is shown to the right at an expanded timescale. Right: Examples of mini-bursts consisting of varying numbers of action potentials recorded from the same SGN.

(H) Plots of the mini-burst rate (n = 8 cells) and percentage of mini-burst events (n = 7 cells) that contained more than one action potential (multiplets) during spontaneous activity in control, + CPP, and wash conditions. One-way repeated-measures ANOVA followed by Tukey's test; n.s., not significant, $p \geq 0.05$; *$p < 0.05$. Data show values from individual cells (gray) and mean ± SEM for all cells (black).

(I) Graph of the percentage of spontaneous mini-bursts containing different numbers of action potentials recorded in control, + CPP, and wash conditions. n = 7 cells; one-way repeated-measures ANOVA followed by Tukey's test for quantification of singlets, doublets, and triplets, and Friedman's ANOVA followed by Dunn's test for quantification of quadruplets and quintuplets and beyond; n.s., not significant, $p \geq 0.05$; *$p < 0.05$. Data show mean + SEM for all cells. See also Figures S6 and S7.

that NMDAR activation increases the probability of SGN firing. To test this hypothesis, we monitored EPSP-action potential coupling in 1.3 mM Mg^{2+}-containing ACSF. In control conditions, 80% of EPSPs triggered action potentials in SGNs, whereas in CPP this coupling was reduced to 61% (Figures 5D and 5E). Notably, our findings suggest that the efficiency of spike generation at this age is high, comparable to that observed after hearing onset (Rutherford et al., 2012; Siegel, 1992), in contrast to recordings from boutons at this age, where only 18% of EPSPs led to action potentials (Yi et al., 2010). Preservation of NMDARs during somatic recordings may contribute to this enhanced EPSP-spike coupling. Given the high probability with which

EPSPs elicit action potentials in SGNs, it is expected that the Mg^{2+} block of NMDARs would be relieved during most synaptic events. Indeed, subtracting the average action potential waveforms in control and CPP (in 1.3 Mg^{2+} ACSF) revealed a slow CPP-sensitive depolarization (Figure 5F), demonstrating that NMDARs contribute substantial postsynaptic depolarization and increase the probability of SGN firing.

To examine how repetitive firing of SGNs is influenced by NMDAR activation, we binned mini-bursts by their spike number: singlets, doublets, triplets, quadruplets, and quintuplets-and-beyond (Figure 5G). NMDAR inhibition reduced the number of mini-bursts (Figure 5H), consistent with the reduction in overall excitability of SGNs (Figures 5A–5C). Moreover, the percentage of multiplets in each burst decreased and the percentage of isolated singlets increased when NMDARs were inhibited (Figures 5H and 5I). These results indicate that NMDARs also promote repetitive firing of SGNs in response to each IHC Ca^{2+} spike. However, NMDAR activity alone was not sufficient to excite SGNs in 1.3 mM Mg^{2+} ACSF but was able to induce SGN firing when Mg^{2+} was eliminated (Figure S7), indicating that AMPARs provide crucial initial depolarization necessary to trigger action potentials and dislodge Mg^{2+} from NMDARs under physiological conditions.

NMDARs Enhance the Overall Excitation and Correlated Spontaneous Activity of SGNs

Release of ATP from ISCs triggers activation of groups of neighboring IHCs (Tritsch and Bergles, 2010; Tritsch et al., 2007), providing a means to synchronize activity of IHCs that will ultimately respond to similar frequencies of sound. To determine if NMDARs promote the transfer of this correlated activity from IHCs to groups of SGNs, we monitored the coincident activity of multiple SGNs by expressing GCaMP3 throughout the cochlea in *Pax2-Cre*; *R26-lsl-GCaMP3* mice. GCaMP3 was expressed by supporting cells, IHCs, and SGNs in these mice (Figures 6A and 6B), enabling simultaneous detection of activity in both Kölliker's organ and the spiral ganglion (Figure 6C). Time-lapse imaging revealed that supporting cells in Kölliker's organ exhibited transient increases in Ca^{2+} that were spatially and temporally correlated with Ca^{2+} elevations in the spiral ganglion (Figures 6C and 6D; Movie S2). Moreover, larger Ca^{2+} rises in Kölliker's organ were correlated with larger Ca^{2+} transients in the spiral ganglion (correlation of the peak amplitude of events: $n = 63$, $r = 0.46$, $p < 0.01$, Pearson's two-tail test). Inhibition of glutamate receptors with NBQX and CPP did not affect the frequency or amplitude of spontaneous Ca^{2+} transients in Kölliker's organ but abolished the synchronized activity of SGNs (Figures 6C and 6E), as expected if supporting cells induce SGN activity indirectly by depolarizing IHCs.

Individual SGNs exhibited distinct patterns of spontaneous activity at this age. During some events, neighboring SGNs showed coincident activity, while in others their activity was uncorrelated (Figure 6F). This behavior is expected, as ATP is released from discrete locations in Kölliker's organ, resulting in recruitment of different IHCs during each event. In ACSF containing Mg^{2+} (1.3 mM), application of CPP reduced the frequency, peak amplitude, and integral of Ca^{2+} transients in individual SGNs (Figures 6G and 6H), suggesting that both the firing rate and number of action potentials within each spontaneous burst were reduced by NMDAR block, in accordance with electrophysiological recordings (see Figure 5). Inhibition of NMDARs also reduced the frequency of spontaneous multi-cellular Ca^{2+} events and the number of SGNs activated during each event (Figures 7A and 7B; Movie S3). Because CPP does not affect activation of supporting cells (Figures S5A–S5C), the excitability of IHCs (Figures S5D and S5E), or the frequency of glutamate release from IHCs (Figure 3), these results indicate that synaptic activation of NMDARs markedly enhance global SGN activity. NMDARs also increase the density of active neurons during each spontaneous event, shown by the greater reduction in the probability of SGN activation with distance from the site of event initiation (the neuron where activity was first observed) when NMDARs were inhibited with CPP (Figures 7C and 7D), resulting in a more sparse activation of SGNs along the tonotopic axis. These population measurements indicate that NMDARs not only shape the firing behavior of individual SGNs but also promote the correlated activity of neighboring SGNs that receive input from similar frequency domains.

NMDARs Promote Survival of SGNs

Elimination of glutamatergic signaling between IHCs and SGNs reduces the number of SGNs and the size of the cochlear nucleus (Seal et al., 2008), indicating that synaptic activity plays an important role in enhancing the survival and integration of SGNs. To determine whether NMDARs contribute to activity-dependent survival of SGNs in the developing cochlea, we generated conditional NMDAR knockout (KO) mice by selectively removing GluN1, an obligatory NMDAR subunit, from a subset of SGNs ($Avil^{Cre}$; $GluN1^{fl/fl}$; *Z/EG*) while preserving NMDAR expression in neurons within central auditory centers (Hasegawa et al., 2007). GluN1 Het and WT SGNs were comparable in their physiological properties, baseline current fluctuations, sensitivity to exogenous NMDA, sEPSC decay tau, and changes induced by CPP application (Figures S8C and S8D). However, GluN1 KO SGNs exhibited less baseline channel noise and did not respond to somatic NMDA application (Figures 8A and 8C), and their sEPSCs had a single-exponential decay that was not altered by application of CPP (Figures 8B and 8C), indicating that these neurons lacked functional NMDARs. The effect of CPP on EPSC decay tau was smaller in these mouse neurons (20% reduction in mouse GluN1 Het SGNs versus 50% reduction in rat SGNs, see Figure 3), perhaps reflecting species differences in NMDAR subunit expression, absolute NMDAR expression level, or EPSC filtering through the dendrite.

To evaluate the effect of NMDARs on SGN integration in vivo, we isolated cochleae from GluN1 Het and KO mice at P30, after the auditory system reaches functional maturity (Sanes and Constantine-Paton, 1985; Wu and Oertel, 1987). Cochleae were serially sectioned from apex to base (Figure 8D) and immunostained, and GFP^+ SGNs were counted (Figure 8E). In GluN1 KO mice there were 34% fewer GFP^+ SGNs compared to cochleae from GluN1 Het mice (Figure 8F), and this reduction was observed in both base and middle regions of the cochlea (Base, 31% reduction; Middle, 42% reduction); too few GFP^+ neurons were present in the apex to analyze. As this conditional KO strategy targets only a small subset of SGNs without manipulating central

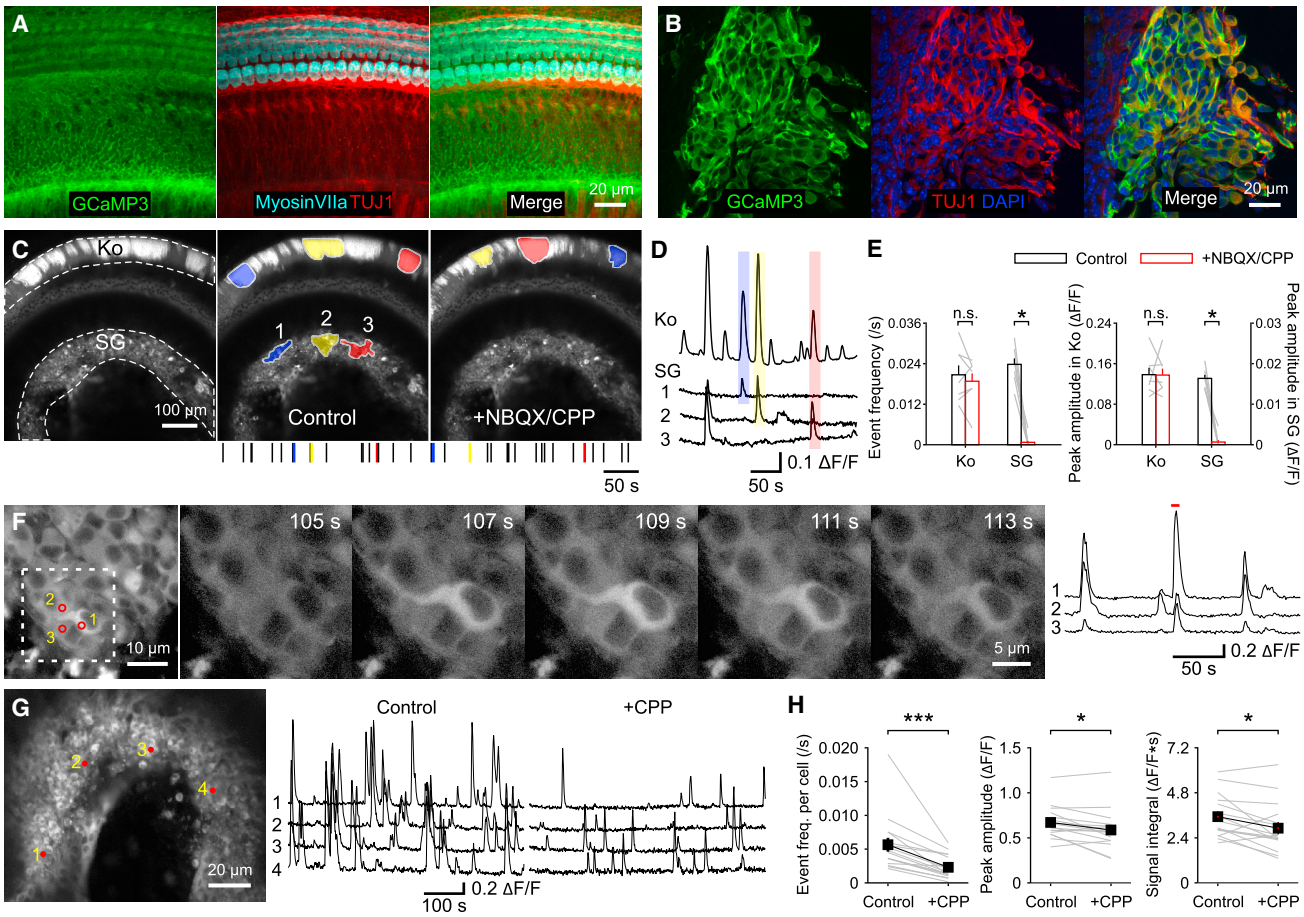

Figure 6. NMDAR Activation Enhances Spontaneous Activity in Individual SGNs

(A and B) Inner sulcus (A) and spiral ganglion (B) of the cochlea from a P5 *Pax2-Cre*; *R26-lsl-GCaMP3* mouse.

(C) Imaging of spontaneous Ca^{2+} transients in the cochlea of a P6 *Pax2-Cre*; *R26-lsl-GCaMP3* mouse. Left: Maximum intensity projection of fluorescence changes in the control condition recorded continuously for 300 s. Middle: Maximum intensity projection image overlaid with maximum activated area of three spontaneous events that appeared in both Kölliker's organ (Ko) and the spiral ganglion (SG). A raster plot indicating the timing of spontaneous events in Kölliker's organ is shown at the bottom, with the three examples shown above highlighted by their corresponding colors. Right: Maximum intensity projection of fluorescence changes for 300 s in NBQX + CPP (both at 20 μM), overlaid with maximum activated area of three spontaneous events that appeared in Kölliker's organ. A raster plot indicating the timing of spontaneous events in Kölliker's organ is shown at the bottom, with the three examples shown above highlighted by their corresponding colors.

(D) Intensity versus time plot for GCaMP3 fluorescence in Kölliker's organ (Ko) and regions of SG shown in (C) with the three spontaneous Ca^{2+} transients in the control condition ([C], Middle) highlighted with their corresponding colors.

(E) Plots of spontaneous Ca^{2+} event frequency and peak amplitude of Ca^{2+} transients in Kölliker's organ and the spiral ganglion in control (white) and NBQX + CPP (red). n = 7 cochleae; paired-sample t test for Kölliker's organs and paired-sample Wilcoxon signed ranks test for spiral ganglia; n.s., not significant, $p \geq 0.05$; *$p < 0.05$. Data show average values from each cochlea (gray lines) and mean + SEM for all cochleae (bars).

(F) Ca^{2+} imaging from individual SGN somata. Left: Maximum intensity projection of fluorescence changes in the spiral gangion from a P5 *Pax2-Cre*; *R26-lsl-GCaMP3* mouse recorded for 300 s. Numbered circles show ROIs used for fluorescence intensity measurements at right. Middle: Individual images for the area delineated at left (dashed white square) at higher magnification showing a Ca^{2+} transient in SGN somata. Right: Intensity versus time plot for the three SGN somata highlighted at left. Red line highlights the Ca^{2+} transient illustrated in the individual images (Middle).

(G) Ca^{2+} imaging of spontaneous activity in the whole spiral ganglion. Left: Maximum intensity projection image of fluorescence changes in the spiral ganglion from a P4 *Pax2-Cre*; *R26-lsl-GCaMP3* mouse recorded for 300 s in the control condition. Numbered circles show ROIs used for fluorescence intensity measurements. Right: Intensity versus time plots for the four SGN somata shown at left in control and + CPP (20 μM) conditions.

(H) Plots of the spontaneous event frequency per neuron, the peak amplitude, and integral of individual Ca^{2+} events in control and + CPP conditions. n = 16 cochleae; paired-sample t test; *$p < 0.05$; ***$p < 0.001$. Data show average values from each cochlea (gray) and mean ± SEM for all cochleae (black).

See also Movie S2.

neurons, these data suggest that NMDAR activation promotes SGN survival in a cell-autonomous manner. Consistent with this hypothesis, repetitive imaging of SGNs in cultured cochleae from P3–P5 *Avil*^{Cre}; *R26-lsl-tdTomato* mice (Figures 8G and 8H) revealed that chronic blockade of NMDARs over 6 days accelerated the death of type I SGNs by ~32%, whereas the

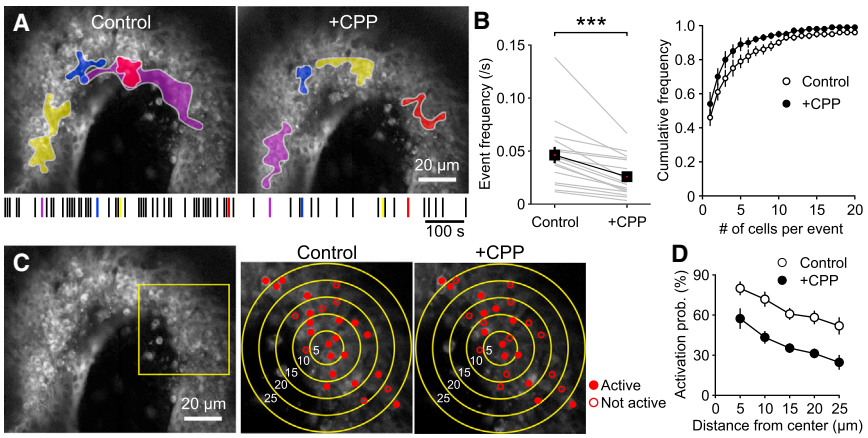

Figure 7. NMDAR Activation Promotes Coincidental Activation of Neighboring SGNs

(A) Maximum intensity projections of fluorescence changes in the spiral ganglion recorded for 300 s in control and + CPP overlaid with maximum activated area of four spontaneous events for both conditions. A raster plot of the timing of spontaneous events in the spiral ganglion is shown at the bottom, with the four examples shown above highlighted by their corresponding colors.

(B) Left: Plot of the correlated spontaneous event frequency in control and + CPP. n = 16 cochleae; paired-sample t test; ***p < 0.001. Data show average values from each cochlea (gray) and mean ± SEM for all cochleae (black). Right: Cumulative frequency distribution of the number of activated SGNs per spontaneous event in control (open) and + CPP (filled) conditions. n = 16 cochleae; two-sample Kolmogorov-Smirnov test; p = 0.03. Data show mean ± SEM for all cochleae.

(C) Maximum intensity projection image of the spinal ganglion (left) showing active (filled) and not active (open) SGNs during single spontaneous events in control and + CPP. Higher magnification images at right were taken from area outlined by yellow square in left panel. Concentric circles indicate 5, 10, 15, 20, and 25 μm away from the location of the first responding SGN.

(D) Plot of activation probability of SGNs versus the distance from location of the first responding SGN in control (open) and + CPP (filled). n = 7 cochleae; two-way repeated-measures ANOVA followed by Bonferroni test; p < 0.001. Data show mean ± SEM for all cochleae.

See also Movie S3.

survival of type II SGNs was unaffected (Figures 8H and 8I). As there are no synaptic connections between SGNs, and SGNs are the sole neurons (now lacking central projections) in these explants, these results indicate that NMDAR activation promotes survival of type I SGNs, independent of feedback from higher-order brain regions.

DISCUSSION

IHCs exhibit robust spontaneous activity in the form of bursts of Ca^{2+} action potentials before hearing onset, which induce correlated, repetitive firing of SGNs residing in similar frequency domains of the cochlea. How IHCs promote these intense periods of activity in developing SGNs is not known. Here we show that nascent synapses between IHCs and SGNs during the prehearing period contain functional NMDARs that markedly prolong synaptic currents, enhance postsynaptic depolarization, and increase the probability of action potential generation. As a result, NMDARs elevate the overall activity of SGNs, enhance their repetitive firing in response to each IHC Ca^{2+} spike, and expand the number of SGNs that are activated during each spontaneous event. Loss of NMDAR signaling impaired SGN survival, reducing the number of SGNs that stably integrated within the spiral ganglion. These studies reveal that spontaneous activity in the prehearing cochlea promotes maturation of the neural pathway responsible for encoding sound through periodic activation of NMDARs in SGNs.

Patterned Spontaneous Activity in the Developing Auditory System

Unlike central synapses, where integration from multiple synapses is required to bring a target neuron to the firing threshold, each multivesicular (Grant et al., 2010) or large uniquantal (Chapochnikov et al., 2014) release event at IHC-SGN synapses provides sufficient depolarization to induce action potentials in SGNs (Figures 5D and 5E). This strong depolarization would be expected to dislodge Mg^{2+} from NMDAR channels, allowing these receptors to prolong depolarization and enhance postsynaptic Ca^{2+} influx during each event. Another unusual aspect of this synapse is that it amplifies IHC activity by allowing each presynaptic Ca^{2+} spike to induce multiple action potentials in the postsynaptic SGN (Tritsch et al., 2010). Our results indicate that NMDAR activation plays an important role in enabling this repetitive firing by extending the period of depolarization. Remarkably, the pattern of activity exhibited by SGNs at this age, which consists of a discrete series of minibursts repeated at an interval set by the frequency of IHC Ca^{2+} spikes, is preserved as it passes through central auditory nuclei. Although the function of this stereotyped repetitive firing, which resembles theta-burst activity, is not known, it may facilitate propagation of activity through immature synapses that exhibit low or moderate release probabilities (Goutman and Glowatzki, 2011; Müller et al., 2010), enable activation of perisynaptic receptors (Carter and Regehr, 2000), and extend the window of opportunity for stabilizing synaptic inputs that exhibit similar patterns of activity.

NMDAR Expression in the Mammalian Cochlea

Transmission at IHC-SGN synapses is mediated by the release of glutamate from ribbon terminals (Glowatzki and Fuchs, 2002; Seal et al., 2008). The composition of glutamate receptors responsible for SGN activation has been investigated through analysis of RNA (RT-PCR, in situ hybridization, and microarray/RNaseq) and protein expression (immunocytochemistry and immunoelectron microscopy), which indicate that a variety of AMPA (GluA2–4), kainate (GluK1) and NMDAR (GluN1 and 2A) subunits are expressed by SGNs (Niedzielski and Wenthold, 1995; Safieddine and Eybalin, 1992), and NMDARs have been reported to be transiently expressed by SGNs during the first

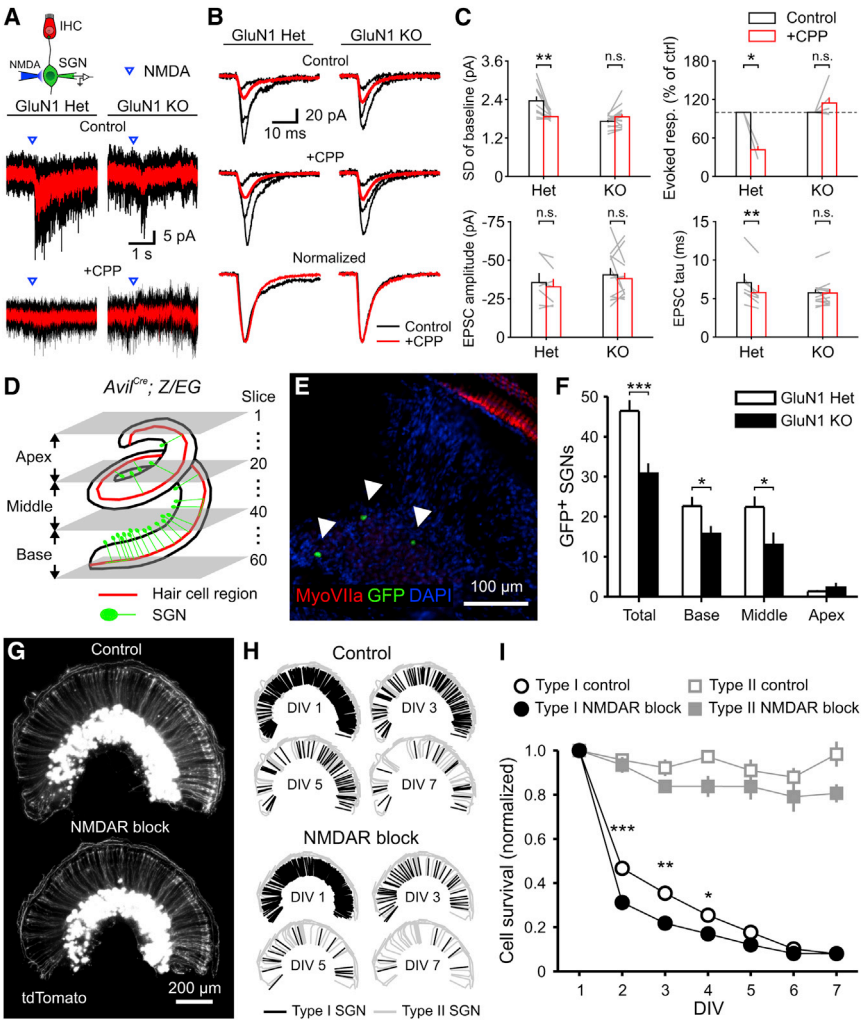

Figure 8. NMDAR Activation Promotes SGN Survival

(A) Upper: Diagram of the recording configuration. Lower: Inward currents triggered by somatic applications of NMDA (20 ms, 0.5 mM) in the presence of TTX (1 μM), recorded from GFP$^+$ SGNs in P4-5 *Avil*^{Cre}; *GluN1*$^{fl/+}$; *Z/EG* (GluN1 Het) and *Avil*^{Cre}; *GluN1*$^{fl/fl}$; *Z/EG* (GluN1 KO) cochleae. Average responses to NMDA (red) are superimposed on individual responses (black). [CPP] = 20 μM.

(B) sEPSCs recorded from GluN1 Het and KO SGNs in control and + CPP conditions. Upper: Average sEPSCs (red) superimposed on three individual sEPSCs (black). Lower: Normalized average sEPSCs in control (black) and + CPP (red) conditions.

(C) Plots of the SD of baseline current fluctuations (n = 10 (Het) and 14 (KO) cells), evoked response by NMDA (n = 3 [Het] and 6 [KO] cells), sEPSC peak amplitude, and weighted tau of decay (n = 6 [Het] and 12 [KO] cells) in control (white) and + CPP (red) conditions. Paired-sample t test; n.s., not significant, $p \geq 0.05$; *$p < 0.05$; **$p < 0.01$. Data show average values from each cell (gray lines) and mean + SEM for all cells (bars).

(D) Diagram showing the method used to count GFP$^+$ SGNs in *Avil*^{Cre}; *Z/EG* cochleae by serial-sectioning at 20 μm per slice. The division of subregions is shown to the left and slice number is shown to the right.

(E) Single immunostained section from a P33 GluN1 Het cochlea (Base, Slice number: 45). Arrowheads indicate somata of GFP$^+$ SGNs.

(F) Graph of the number of GFP$^+$ SGNs in GluN1 Het (open bars, n = 9 mice) and GluN1 KO (filled bars, n = 11 mice) cochleae. Two sample t test without assuming equal variance; *$p < 0.05$; ***$p < 0.001$. Data are shown as mean + SEM for all cochleae.

(G) Fluorescence image of *Avil*^{Cre}; *tdT* cochlea cultures (P3–P4 DIV 1) incubated in control media (upper) or media containing NMDAR blockers (lower, 50 μM MK-801 + 20 μM CPP).

(H) Schematic showing the distribution of type I (black) and type II (gray) SGN dendrites labeled by tdTomato in (G) on DIV 1, 3, 5, and 7 in control and NMDAR block conditions.

(I) Survival curves of type I (black) and type II (gray) SGNs in control (open symbols, n = 6 cochleae) and NMDAR block (filled symbols, n = 5 cochleae) conditions. Two-way ANOVA with repeated-measures in one factor followed by Bonferroni test; no asterisk, not significant, $p \geq 0.05$; *$p < 0.05$; **$p < 0.01$; ***$p < 0.001$. Data show mean ± SEM for all cochleae.

See also Figure S8.

2 weeks in rats (Knipper et al., 1997). However, direct functional evidence for participation of NMDARs in synaptic transmission at this first synapse in the auditory pathway has been elusive. Our results indicate that functional NMDARs are expressed by SGNs in cochlea before hearing onset and that these receptors are reliably activated by synaptic glutamate release from IHCs. Although all SGNs exhibited somatic responses to NMDA, not all terminals exhibited NMDAR-mediated Ca^{2+} transients (see Figure 4D), and the NMDAR-mediated component varied among individual SGNs, as shown by the variability in the decay kinetics of sEPSCs (see Figure S4D). Furthermore, the firing of some SGNs was blocked by AMPA receptor antagonists alone (7/25 SGNs), suggesting that the NMDAR current is not always of sufficient magnitude to induce postsynaptic excitation. This variability in contribution of NMDARs to SGN excitation may arise from selecting cells in different states of dendritic maturation. Indeed, previous studies indicated that NMDARs are expressed transiently in the developing inner ear (Knipper et al., 1997). It may also reflect the physiological diversity of SGNs, which vary dramatically in their rates of spontaneous activity in vivo (Taberner and Liberman, 2005).

Roles of NMDARs in the Developing Cochlea

NMDARs have been shown to play a prominent role in neural development by regulating cell survival, dendritic and axonal arborization, and synapse formation (Collingridge et al., 2004; Contestabile, 2000; Ewald and Cline, 2009). Hippocampal CA1 pyramidal neurons depleted of GluN1 receive greater glutamatergic synaptic input (Adesnik et al., 2008), an effect attributed to the occupation of additional receptor sites in the postsynaptic

membrane by AMPA receptors when NMDARs are removed (Gray et al., 2011). In accordance with studies in the brain, glutamatergic synapses were still formed between IHCs and SGNs without NMDARs, but there was a trend toward larger amplitude sEPSCs in GluN1 KO SGNs (see Figure 8C), suggesting that there may be more territory available to AMPARs at these ribbon synapses.

The formation of circuits during early development is accompanied by widespread loss of neurons that fail to establish appropriate connections (Kuan et al., 2000; Nijhawan et al., 2000). Survival of neurons during this period is promoted by activity (Mennerick and Zorumski, 2000), and systemic administration of the NMDAR antagonist MK-801 during the first 2 postnatal weeks in rats triggers widespread neuronal apoptosis (Ikonomidou et al., 1999), suggesting that NMDAR activation promotes neuronal survival during a critical period. However, these studies could not exclude the possibility that the effects may arise from emergent, abnormal patterns of activity induced by NMDAR inhibition at early ages (Homayoun and Moghaddam, 2007; Jackson et al., 2004). Thus, a cell-autonomous role for NMDAR signaling in neuronal survival has not been examined in vivo. Previous studies suggest that synaptic activity promotes SGN integration, as the size of the spiral ganglion is reduced in mice that lack vGluT3 (Seal et al., 2008). Our results show that disrupting NMDAR expression in a small subset of SGNs in vivo led to a 34% decrease in their survival (see Figure 8F), comparable to the extent of SGN loss observed in vGluT3 null mice, indicating that NMDAR activation promotes SGN integration.

Previous studies suggest that NMDARs may also contribute to signaling in the mature cochlea: GluN1 subunit immunostaining is robust around the base of IHCs in adult rats (Ruel et al., 2008); infusion of the NMDAR antagonist 2-amino-5-phosphonovalerate (APV) through the perilymphatic scalae reduced compound action potentials recorded from the auditory nerve (Puel et al., 1991); and systemic infusion of MK-801 reduced swelling of SGN dendrites following exposure to intense sound (Duan et al., 2000). Although the slow activation and deactivation kinetics of NMDARs would be expected to limit the fidelity of sound encoding at high frequencies, prolonged depolarization could be counteracted by expression of leak channels to maintain a low membrane resistance and HCN channels to shorten EPSPs in SGN dendritic terminals (Chen and Davis, 2006). A transition from GluN2B- to GluN2A-containing NMDARs similar to the developmental change observed at central synapses (Cull-Candy et al., 2001) would also be expected to shorten EPSP time course and restrict plasticity. Direct assessment of the role of NMDARs in sound encoding and cochlear trauma in the mature cochlea will require development of a SGN-specific CreER mouse line that enables selective deletion of GluN1 from adult SGNs.

EXPERIMENTAL PROCEDURES

Animals

All experiments were performed in accordance with protocols approved by the Animal Care and Use Committee at Johns Hopkins University. P0 to P7 Sprague Dawley rat (Charles River Laboratories) and mouse pups were used for recording and imaging.

Electrophysiology

Recordings were performed at room temperature as described previously (Tritsch et al., 2007). Currents and potentials were recorded using a MultiClamp 700A amplifier (Molecular Devices) with pClamp9 software, and data were analyzed using Clampfit (Molecular Devices), Origin (OriginLab), MiniAnalysis (Synaptosoft), and custom routines written in Matlab.

Imaging

GCaMP3 fluorescence was imaged with a laser scanning confocal microscope (LSM 710; Zeiss) using a 20× water-immersion objective. In vitro cell survival experiments were performed using an inverted light microscope (Axio Observer; Zeiss) with a 10× objective. Data were analyzed using ImageJ (NIH).

Statistics

Data are expressed as mean ± SEM, and statistical tests were performed as indicated in Table S1, with significance determined by p value < 0.05.

SUPPLEMENTAL INFORMATION

Supplemental Information includes eight figures, one table, three movies, and Supplemental Experimental Procedures and can be found with this article online at http://dx.doi.org/10.1016/j.neuron.2015.12.016.

AUTHOR CONTRIBUTIONS

Y.Z.-H. and D.E.B. conceived the project, designed the experiments, and wrote the manuscript. Y.Z.-H. conducted experiments and analyzed the data. A.A. generated and characterized the *R26-lsl-GCaMP3* mice. M.M. provided the *GluN1* floxed mice.

ACKNOWLEDGMENTS

We thank Yin Liu (Stanford University) for help in identifying Cre expression in SGNs of $Avil^{Cre}$ mice, Andrew Groves (Baylor College of Medicine) for providing *Pax2-Cre* mice, Fan Wang (Duke University) for providing $Avil^{Cre}$ mice, and Bryan M. Hooks (University of Pittsburgh) for writing Matlab codes to analyze SGN mini-bursts. Nicolas X. Tritsch (Harvard Medical School), Huaqiang Fang, Han Chin Wang, Yung-Tian Gau, and Travis Babola provided technical assistance. We also thank members of the Bergles laboratory for helpful discussions and Peter Z. Hooks for his timely support. A.A. was supported by a postdoctoral fellowship from the National Multiple Sclerosis Society. This work was supported by grants from the NIH (DC008860, MH100024, and NS050274).

Received: February 19, 2015
Revised: October 8, 2015
Accepted: November 24, 2015
Published: January 7, 2016; corrected online: January 20, 2016

REFERENCES

Adesnik, H., Li, G., During, M.J., Pleasure, S.J., and Nicoll, R.A. (2008). NMDA receptors inhibit synapse unsilencing during brain development. Proc. Natl. Acad. Sci. USA *105*, 5597–5602.

Beutner, D., and Moser, T. (2001). The presynaptic function of mouse cochlear inner hair cells during development of hearing. J. Neurosci. *21*, 4593–4599.

Blankenship, A.G., and Feller, M.B. (2010). Mechanisms underlying spontaneous patterned activity in developing neural circuits. Nat. Rev. Neurosci. *11*, 18–29.

Carter, A.G., and Regehr, W.G. (2000). Prolonged synaptic currents and glutamate spillover at the parallel fiber to stellate cell synapse. J. Neurosci. *20*, 4423–4434.

Chapochnikov, N.M., Takago, H., Huang, C.H., Pangršič, T., Khimich, D., Neef, J., Auge, E., Göttfert, F., Hell, S.W., Wichmann, C., et al. (2014). Uniquantal release through a dynamic fusion pore is a candidate mechanism of hair cell exocytosis. Neuron *83*, 1389–1403.

Chen, W.C., and Davis, R.L. (2006). Voltage-gated and two-pore-domain potassium channels in murine spiral ganglion neurons. Hear. Res. *222*, 89–99.

Cho, S., and von Gersdorff, H. (2014). Proton-mediated block of Ca2+ channels during multivesicular release regulates short-term plasticity at an auditory hair cell synapse. J. Neurosci. *34*, 15877–15887.

Clause, A., Kim, G., Sonntag, M., Weisz, C.J., Vetter, D.E., Rűbsamen, R., and Kandler, K. (2014). The precise temporal pattern of prehearing spontaneous activity is necessary for tonotopic map refinement. Neuron *82*, 822–835.

Collingridge, G.L., Isaac, J.T., and Wang, Y.T. (2004). Receptor trafficking and synaptic plasticity. Nat. Rev. Neurosci. *5*, 952–962.

Contestabile, A. (2000). Roles of NMDA receptor activity and nitric oxide production in brain development. Brain Res. Brain Res. Rev. *32*, 476–509.

Cull-Candy, S.G., and Usowicz, M.M. (1987). Multiple-conductance channels activated by excitatory amino acids in cerebellar neurons. Nature *325*, 525–528.

Cull-Candy, S.G., Brickley, S., and Farrant, M. (2001). NMDA receptor subunits: diversity, development and disease. Curr. Opin. Neurobiol. *11*, 327–335.

da Silva, S., Hasegawa, H., Scott, A., Zhou, X., Wagner, A.K., Han, B.X., and Wang, F. (2011). Proper formation of whisker barrelettes requires periphery-derived Smad4-dependent TGF-beta signaling. Proc. Natl. Acad. Sci. USA *108*, 3395–3400.

Duan, M., Agerman, K., Ernfors, P., and Canlon, B. (2000). Complementary roles of neurotrophin 3 and a N-methyl-D-aspartate antagonist in the protection of noise and aminoglycoside-induced ototoxicity. Proc. Natl. Acad. Sci. USA *97*, 7597–7602.

Ewald, R.C., and Cline, H.T. (2009). NMDA Receptors and Brain Development.

Felix, D., and Ehrenberger, K. (1990). A microiontophoretic study of the role of excitatory amino acids at the afferent synapses of mammalian inner hair cells. Eur. Arch. Otorhinolaryngol. *248*, 1–3.

Gideons, E.S., Kavalali, E.T., and Monteggia, L.M. (2014). Mechanisms underlying differential effectiveness of memantine and ketamine in rapid antidepressant responses. Proc. Natl. Acad. Sci. USA *111*, 8649–8654.

Glowatzki, E., and Fuchs, P.A. (2002). Transmitter release at the hair cell ribbon synapse. Nat. Neurosci. *5*, 147–154.

Goforth, P.B., Ren, J., Schwartz, B.S., and Satin, L.S. (2011). Excitatory synaptic transmission and network activity are depressed following mechanical injury in cortical neurons. J. Neurophysiol. *105*, 2350–2363.

Goutman, J.D., and Glowatzki, E. (2011). Short-term facilitation modulates size and timing of the synaptic response at the inner hair cell ribbon synapse. J. Neurosci. *31*, 7974–7981.

Grant, L., Yi, E., and Glowatzki, E. (2010). Two modes of release shape the postsynaptic response at the inner hair cell ribbon synapse. J. Neurosci. *30*, 4210–4220.

Gray, J.A., Shi, Y., Usui, H., During, M.J., Sakimura, K., and Nicoll, R.A. (2011). Distinct modes of AMPA receptor suppression at developing synapses by GluN2A and GluN2B: single-cell NMDA receptor subunit deletion in vivo. Neuron *71*, 1085–1101.

Hasegawa, H., Abbott, S., Han, B.X., Qi, Y., and Wang, F. (2007). Analyzing somatosensory axon projections with the sensory neuron-specific Advillin gene. J. Neurosci. *27*, 14404–14414.

Homayoun, H., and Moghaddam, B. (2007). NMDA receptor hypofunction produces opposite effects on prefrontal cortex interneurons and pyramidal neurons. J. Neurosci. *27*, 11496–11500.

Ikonomidou, C., Bosch, F., Miksa, M., Bittigau, P., Vöckler, J., Dikranian, K., Tenkova, T.I., Stefovska, V., Turski, L., and Olney, J.W. (1999). Blockade of NMDA receptors and apoptotic neurodegeneration in the developing brain. Science *283*, 70–74.

Jackson, M.E., Homayoun, H., and Moghaddam, B. (2004). NMDA receptor hypofunction produces concomitant firing rate potentiation and burst activity reduction in the prefrontal cortex. Proc. Natl. Acad. Sci. USA *101*, 8467–8472.

Jagger, D.J., and Housley, G.D. (2002). A-type potassium currents dominate repolarisation of neonatal rat primary auditory neurones in situ. Neuroscience *109*, 169–182.

Johnson, S.L., Eckrich, T., Kuhn, S., Zampini, V., Franz, C., Ranatunga, K.M., Roberts, T.P., Masetto, S., Knipper, M., Kros, C.J., and Marcotti, W. (2011). Position-dependent patterning of spontaneous action potentials in immature cochlear inner hair cells. Nat. Neurosci. *14*, 711–717.

Káradóttir, R., Cavelier, P., Bergersen, L.H., and Attwell, D. (2005). NMDA receptors are expressed in oligodendrocytes and activated in ischaemia. Nature *438*, 1162–1166.

Kirkby, L.A., Sack, G.S., Firl, A., and Feller, M.B. (2013). A role for correlated spontaneous activity in the assembly of neural circuits. Neuron *80*, 1129–1144.

Knipper, M., Köpschall, I., Rohbock, K., Köpke, A.K., Bonk, I., Zimmermann, U., and Zenner, H. (1997). Transient expression of NMDA receptors during rearrangement of AMPA-receptor-expressing fibers in the developing inner ear. Cell Tissue Res. *287*, 23–41.

Kuan, C.Y., Roth, K.A., Flavell, R.A., and Rakic, P. (2000). Mechanisms of programmed cell death in the developing brain. Trends Neurosci. *23*, 291–297.

Lu, C.C., Appler, J.M., Houseman, E.A., and Goodrich, L.V. (2011). Developmental profiling of spiral ganglion neurons reveals insights into auditory circuit assembly. J. Neurosci. *31*, 10903–10918.

MacDermott, A.B., Mayer, M.L., Westbrook, G.L., Smith, S.J., and Barker, J.L. (1986). NMDA-receptor activation increases cytoplasmic calcium concentration in cultured spinal cord neurones. Nature *321*, 519–522.

MacDonald, J.F., Mody, I., and Salter, M.W. (1989). Regulation of N-methyl-D-aspartate receptors revealed by intracellular dialysis of murine neurones in culture. J. Physiol. *414*, 17–34.

Mennerick, S., and Zorumski, C.F. (2000). Neural activity and survival in the developing nervous system. Mol. Neurobiol. *22*, 41–54.

Müller, M., Goutman, J.D., Kochubey, O., and Schneggenburger, R. (2010). Interaction between facilitation and depression at a large CNS synapse reveals mechanisms of short-term plasticity. J. Neurosci. *30*, 2007–2016.

Niedzielski, A.S., and Wenthold, R.J. (1995). Expression of AMPA, kainate, and NMDA receptor subunits in cochlear and vestibular ganglia. J. Neurosci. *15*, 2338–2353.

Nijhawan, D., Honarpour, N., and Wang, X. (2000). Apoptosis in neural development and disease. Annu. Rev. Neurosci. *23*, 73–87.

Papadia, S., Stevenson, P., Hardingham, N.R., Bading, H., and Hardingham, G.E. (2005). Nuclear Ca2+ and the cAMP response element-binding protein family mediate a late phase of activity-dependent neuroprotection. J. Neurosci. *25*, 4279–4287.

Paukert, M., Agarwal, A., Cha, J., Doze, V.A., Kang, J.U., and Bergles, D.E. (2014). Norepinephrine controls astroglial responsiveness to local circuit activity. Neuron *82*, 1263–1270.

Peng, B.G., Chen, S., and Lin, X. (2003). Aspirin selectively augmented N-methyl-D-aspartate types of glutamate responses in cultured spiral ganglion neurons of mice. Neurosci. Lett. *343*, 21–24.

Puel, J.L., Ladrech, S., Chabert, R., Pujol, R., and Eybalin, M. (1991). Electrophysiological evidence for the presence of NMDA receptors in the guinea pig cochlea. Hear. Res. *51*, 255–264.

Rosenmund, C., and Westbrook, G.L. (1993). Rundown of N-methyl-D-aspartate channels during whole-cell recording in rat hippocampal neurons: role of Ca2+ and ATP. J. Physiol. *470*, 705–729.

Ruel, J., Chabbert, C., Nouvian, R., Bendris, R., Eybalin, M., Leger, C.L., Bourien, J., Mersel, M., and Puel, J.L. (2008). Salicylate enables cochlear arachidonic-acid-sensitive NMDA receptor responses. J. Neurosci. *28*, 7313–7323.

Rutherford, M.A., Chapochnikov, N.M., and Moser, T. (2012). Spike encoding of neurotransmitter release timing by spiral ganglion neurons of the cochlea. J. Neurosci. *32*, 4773–4789.

Safieddine, S., and Eybalin, M. (1992). Co-expression of NMDA and AMPA/kainate receptor mRNAs in cochlear neurones. Neuroreport *3*, 1145–1148.

Safieddine, S., El-Amraoui, A., and Petit, C. (2012). The auditory hair cell ribbon synapse: from assembly to function. Annu. Rev. Neurosci. *35*, 509–528.

Sah, P., Hestrin, S., and Nicoll, R.A. (1989). Tonic activation of NMDA receptors by ambient glutamate enhances excitability of neurons. Science *246*, 815–818.

Sanes, D.H., and Constantine-Paton, M. (1985). The development of stimulus following in the cochlear nerve and inferior colliculus of the mouse. Brain Res. *354*, 255–267.

Savić, N., Lüthi, A., Gähwiler, B.H., and McKinney, R.A. (2003). N-methyl-D-aspartate receptor blockade during development lowers long-term potentiation threshold without affecting dynamic range of CA3-CA1 synapses. Proc. Natl. Acad. Sci. USA *100*, 5503–5508.

Seal, R.P., Akil, O., Yi, E., Weber, C.M., Grant, L., Yoo, J., Clause, A., Kandler, K., Noebels, J.L., Glowatzki, E., et al. (2008). Sensorineural deafness and seizures in mice lacking vesicular glutamate transporter 3. Neuron *57*, 263–275.

Siegel, J.H. (1992). Spontaneous synaptic potentials from afferent terminals in the guinea pig cochlea. Hear. Res. *59*, 85–92.

Sinning, A., and Hübner, C.A. (2013). Minireview: pH and synaptic transmission. FEBS Lett. *587*, 1923–1928.

Taberner, A.M., and Liberman, M.C. (2005). Response properties of single auditory nerve fibers in the mouse. J. Neurophysiol. *93*, 557–569.

Tang, C.M., Dichter, M., and Morad, M. (1990). Modulation of the N-methyl-D-aspartate channel by extracellular H+. Proc. Natl. Acad. Sci. USA *87*, 6445–6449.

Tian, L., Hires, S.A., Mao, T., Huber, D., Chiappe, M.E., Chalasani, S.H., Petreanu, L., Akerboom, J., McKinney, S.A., Schreiter, E.R., et al. (2009). Imaging neural activity in worms, flies and mice with improved GCaMP calcium indicators. Nat. Methods *6*, 875–881.

Traynelis, S.F., Hartley, M., and Heinemann, S.F. (1995). Control of proton sensitivity of the NMDA receptor by RNA splicing and polyamines. Science *268*, 873–876.

Tritsch, N.X., and Bergles, D.E. (2010). Developmental regulation of spontaneous activity in the Mammalian cochlea. J. Neurosci. *30*, 1539–1550.

Tritsch, N.X., Yi, E., Gale, J.E., Glowatzki, E., and Bergles, D.E. (2007). The origin of spontaneous activity in the developing auditory system. Nature *450*, 50–55.

Tritsch, N.X., Rodríguez-Contreras, A., Crins, T.T., Wang, H.C., Borst, J.G., and Bergles, D.E. (2010). Calcium action potentials in hair cells pattern auditory neuron activity before hearing onset. Nat. Neurosci. *13*, 1050–1052.

Tzounopoulos, T., Kim, Y., Oertel, D., and Trussell, L.O. (2004). Cell-specific, spike timing-dependent plasticities in the dorsal cochlear nucleus. Nat. Neurosci. *7*, 719–725.

Usami, S., Matsubara, A., Fujita, S., Shinkawa, H., and Hayashi, M. (1995). NMDA (NMDAR1) and AMPA-type (GluR2/3) receptor subunits are expressed in the inner ear. Neuroreport *6*, 1161–1164.

Wu, S.H., and Oertel, D. (1987). Maturation of synapses and electrical properties of cells in the cochlear nuclei. Hear. Res. *30*, 99–110.

Xia, Z., Dudek, H., Miranti, C.K., and Greenberg, M.E. (1996). Calcium influx via the NMDA receptor induces immediate early gene transcription by a MAP kinase/ERK-dependent mechanism. J. Neurosci. *16*, 5425–5436.

Yi, E., Roux, I., and Glowatzki, E. (2010). Dendritic HCN channels shape excitatory postsynaptic potentials at the inner hair cell afferent synapse in the mammalian cochlea. J. Neurophysiol. *103*, 2532–2543.